Manuscript submitted to
AIMS' Journals
Volume **X**, Number **0X**, XX **200X**

Website: http://AIMsciences.org

pp. **X–XX**

GLOBAL EXISTENCE FOR CHEMOTAXIS WITH FINITE SAMPLING RADIUS

T. Hillen*, K. Painter+, C. Schmeiser**

*University of Alberta, Edmonton T6G 2G1, Canada, thillen@ualberta.ca
+Heriot-Watt University, Edinburgh, EH11 1UF, UK, painter@ma.hw.ac.uk
**University of Vienna, Vienna, Austria, christian.schmeiser@univie.ac.at

(Communicated by Aim Sciences)

Abstract. Migrating cells measure the external environment through receptor-binding of specific chemicals at their outer cell membrane. In this paper this non-local sampling is incorporated into a chemotactic model. The existence of global bounded solutions of the non-local model is proven for bounded and unbounded domains in any space dimension. According to a recent classification of spikes and plateaus, it is shown that steady state solutions cannot be of spike-type. Finally, numerical simulations support the theoretical results, illustrating the ability of the model to give rise to pattern formation. Some biologically relevant extensions of the model are also considered.

1. **Introduction.** Chemotaxis, the active orientation of cells and organisms along chemical gradients, plays a crucial role in many biological processes, including embryonic development, immunology and cancer growth. Accordingly, a vast amount of research, both experimental and theoretical, has been devoted to understanding the mechanistic basis of chemotaxis.

In 1953, Patlak [28] introduced the first mathematical model for chemotaxis. A similar model was derived by Keller and Segel in 1970 [16], albeit under different assumptions. These pioneering works have initiated an intensive mathematical investigation of the Patlak-Keller-Segel (PKS) model over the last 30 years. Of particular interest is the following special case, which we refer to as the *classical chemotaxis model*:

$$\begin{aligned} u_t &= \nabla \cdot (D_u \nabla u - \chi u \nabla s) \\ s_t &= D_s \Delta s + \alpha u - \beta s. \end{aligned} \tag{1}$$

The function $u(x,t)$ denotes the population density at time t and location x, while $s(x,t)$ denotes the concentration of a chemical signal; in the above model this is produced by the species themselves. The parameters $\chi, \alpha, \beta, D_u, D_s$ are non-negative. The system (1) has been studied on bounded domains with appropriate boundary conditions (Neumann, Dirichlet, Robin etc.) or on unbounded domains (see e.g. Hortsmann [12] and Dolbeault and Perthame [7]). An important feature of the above model lies in its ability to exhibit pattern formation, or "aggregation": an

2000 *Mathematics Subject Classification.* Primary: 92C17 Secondary: 35K10.

Key words and phrases. Chemotaxis, Global Existence, Finite Sampling Radius, Non-local Gradient.

The first author is supported by NSERC, Canada. The second author is partially supported by an NIH integrative cancer biology program grant CA113004. The third author is supported by the Austrian Science Fund and by the Vienna Science and Technology Fund.

example of a typical aggregation pattern for (1) can be found in Figure 3 (a). As such, models based on the above equations have been applied to a wide range of biological pattern formation processes, including mound formation in the slime mold *Dictyostelium*, bacterial pattern formation, animal pigmentation patterns and limb bud patterning ([16, 33, 26, 18]).

In this paper we study a simple modification of the classical chemotaxis model (1), where the gradient sensing term ∇s is replaced by the non-local gradient $\overset{\circ}{\nabla}_\rho\, s$:

$$\begin{aligned} u_t &= \nabla \cdot (D_u \nabla u - \chi u \overset{\circ}{\nabla}_\rho\, s) \\ s_t &= D_s \Delta s + \alpha u - \beta s, \end{aligned} \tag{2}$$

where for $\rho > 0$ the non-local gradient, which was introduced in [22], is defined as

$$\overset{\circ}{\nabla}_\rho\, s(x,t) = \frac{n}{\omega \rho} \int_{S^{n-1}} \sigma s(x + \rho\sigma, t)\, d\sigma, \tag{3}$$

where $\omega = |S^{n-1}|$ and S^{n-1} denotes the $(n-1)$-dimensional unit sphere in $\mathbb{R}^n$. The nonlocal gradient describes sensing of the chemical signal over an effective sampling radius $\rho > 0$.

The model is modified in a straightforward way, when the position domain is not the whole space $\mathbb{R}^n$, but some $\Omega \subset \mathbb{R}^n$:

$$\overset{\circ}{\nabla}_\rho\, s(x,t) = \frac{n}{\omega_\Omega(x) \rho} \int_{S_\Omega^{n-1}(x)} \sigma s(x + \rho\sigma, t)\, d\sigma, \tag{4}$$

with $S_\Omega^{n-1}(x) = \{\sigma \in S^{n-1} :\ x + \rho\sigma \in \Omega\}$ and $\omega_\Omega(x) = |S_\Omega^{n-1}(x)|$.

While the classical chemotaxis model (1) in dimensions 2 or higher is known to exhibit solutions that blow-up in finite time, we show in this paper that the non-local model (2) has global in time solutions on bounded or unbounded domains in any dimension, as long as $\rho > 0$ (Theorem 1). Details behind this model and about the analysis will be given later. First we summarise some results of the classical chemotaxis model (1) relevant to the analysis here.

For (1) on bounded domains it has been shown that the qualitative behaviour of solutions depends strongly on the space dimension. An extensive review article by D. Horstmann, [12], concerning (1) and related models provides greater detail, here we summarise the essentials. In one space dimension, solutions exist globally, a fact only recently proven (Osaki and Yagi [21], see also Hillen and Potapov [10] and Horstmann and Winkler [13]). In Hillen and Potapov [10] numerical and asymptotic arguments have been applied to demonstrate that solutions to (1) in one-dimension typically form spikes. For two-dimensional domains, global existence depends on a threshold: when the initial mass lies below the threshold solutions exist globally, while above the threshold solutions blow up in finite time (see references in Horstmann [12], or the new book of Suzuki [32], and Dolbeault and Perthame [7] for a recent result). Under the biologically relevant cases for aggregation to occur, the initial conditions typically lie above this threshold — hence while the model does predict aggregation, this takes the form of a finite time blow-up.

It is of interest to study biologically relevant and mathematically useful modifications of the classical chemotaxis model (1) that prevent blow-up and allow for global solutions. Several of these regularizations have been studied in the literature, including saturation effects (e.g. Othmer and Stevens [24], Rivero *et al.* [31], Aida *et al.* [1]), volume filling (e.g. Painter and Hillen [25]), attraction-repulsion mechanisms (e.g. Luca *et al.* [17] Renclawowicz and Hillen [30]), cell kinetics (e.g.

Wrzosek [35]), nonlinear motility parameter and nonlinear chemotactic sensitivity (e.g. Horstmann [11]), self similar solutions (e.g. Biler [4]), and non-local effects as studied here. Nonlocal terms appear in the classical chemotaxis model (1) as well, if for the signal equation the quasi steady state assumption is used. In that case, the signal satisfies an elliptic equation, that can be solved using the Greens function for the given domain Ω (see Biler [4]). Then s is expressed as convolution of the Greens function with u, and hence leads to a nonlocal term in the first equation of (1). This modeling differs significantly from the non-local term studied in this paper. Here we assume cells measure their environment along their outer body membrane. The non-local dependence directly relates to the physical realization of a cell. In the Greens-function approach, the nonlocal effect stems from a instantaneous global response of the signal s to the cell distribution u.

As seen for the classical chemotaxis model (1), typical non-trivial solutions form very sharp and thin local maxima (spikes). These spikes remain bounded in 1-D and blow up in n-D, $n \geq 2$. For the volume filling model, for example, typical patterns are of plateau-type (see Painter and Hillen [25], Dolak and Schmeiser [6]). In Hillen [8] a classification of spikes versus plateaus is given, using the non-local gradient (3). We show in this paper that solutions of (2) are global in time and steady states are of plateau-type. We prove that the non-local chemotaxis model (2) cannot have spike steady states.

The paper is organized as follows. In section 2 we derive the finite sampling radius model from biological observations. We properly define the nonlocal gradient and we show some basic properties of $\overset{\circ}{\nabla}_\rho$. In section 3 we prove global in time existence of solutions to the model (2) in any space dimension. The proof relies on the trace theorem for the nonlocal gradient and the Nash estimate. In section 4 we employ linear stability analysis to determine the conditions under which aggregation is possible, we summarise the classification into spikes and plateaus from [8], and we show that (2) cannot have spike steady states. Moreover, we construct approximate plateau steady states. In section 5 we present numerical simulations for the non-local model (2), illustrate the possibility of pattern formation and the dependence on the sampling radius $\rho > 0$. In particular, we show numerically that as $\rho \to 0$ the solutions become singular (blowup). A rigorous discussion of convergence of solutions for $\rho \to 0$ is not done in this paper. We close the paper with a discussion section 6, where we discuss the significance of our results and give an outlook to future research directions.

2. The Finite Sampling Radius.

While details vary between systems, common to all processes of chemosensitive movement is the detection and response to an external signal. In cells, detection of the external chemoattractant typically occurs through binding to specific membrane receptors, for example Rappel et al. [29] demonstrate that cells polarize in a signal gradient by measuring the actual signal concentration along their body membrane. Incorporating the "sampling radius" into models for chemotaxis thus arises naturally from these considerations: at its most intuitive level it could represent the movement response through signal detection at the cell membrane. In practice, this sampling radius may be many times larger than the physical extent of the cell: studies on the physics of chemoreception by Purcell and Berg [3] indicate that the *effective* sampling volume depends on the time taken for a signal to be processed by a cell, and for realistic parameter values

in *Dictyostelium* this can swell the physical sampling volume by several times [23]. The actual sampling volume can also be affected by cell shape: migrating cells extend a variety of cellular protrusions, including pseudopodia, lamellipodia and filopodia, the latter extending up to 80-100 μm in length.

Such considerations led Othmer and Hillen [22] to propose the inclusion of a finite sampling radius in a model, as defined in (3). In this section we demonstrate how such models can be derived from two different approaches: the first, a phenomenological approach, considers its derivation from a force balance approach, while the latter considers the derivation from a kinetic transport equation.

2.1. **Derivation from Force Balance.** Our phenomenological derivation for a class of non-local models including (2) follows the approach in [27]. Macroscopic movement equations derive from Newton's law by considering the forces exerted by a cell in multiple directions. We assume that the cell density, $u(\mathbf{x}, t)$ follows the general conservation law

$$u_t = -\nabla \cdot J\,,$$

where J is the cell flux, comprising of both a diffusive component, modelling random effects, and a guided component modelling the chemotactic response,

$$J = J_{\text{diffusion}} + J_{\text{chemotaxis}}\,,$$

where we take $J_{\text{diffusion}} = -D_u \nabla u$ for simplicity. Following the approach of [27], we propose a chemotactic flux of the form

$$J_{\text{chemotaxis}} = u\phi F\,,$$

where ϕF represents the *chemotactic velocity* with motility coefficient ϕ (which could incorporate effects due to other chemicals, ECM or cell interactions) and F is the net force generated by the cell in response to the chemical environment. The above follows directly from Newton's law, assuming negligible inertia (reasonable at the low speeds of cell migration) and that drag is proportional to velocity.

The mechanism for force generation varies greatly between cells. In ameoboidal cells such as *Dictyostelium* and leukocytes, force is generated through the creation of adhesive attachments at the cell membrane with the substrate/ECM; such cells frequently extend pseudopods in multiple directions during movement, e.g. Varnum-Finney *et al.* [34]. Under this assumption, a one-dimensional cell centred at x and of radius ρ can generate forces in the positive/negative direction of magnitude $f^{\pm} \equiv f(a(x \pm \rho))$, where a represents the number of adhesive attachments made by the cell. The net force is

$$F = f(a(x+\rho)) - f(a(x-\rho))\,,$$

which, upon substituting into the flux gives,

$$J = -D_u u_x + u\phi(f(s(x+\rho)) - f(s(x-\rho))).$$

Mass conservation thus takes the form

$$u_t = D_u u_{xx} - \left(u\phi(f(a(x+\rho)) - f(a(x-\rho)))\right)_x\,.$$

The extension to higher dimensions is similar. The magnitude of the force in a direction σ ($|\sigma| = 1$) will depend on the number of attachments made at the boundary in that direction,

$$f(\sigma) = f(a(x + \rho\sigma)).$$

Summing over all directions to obtain the net force and substituting into the conservation equation, we obtain a non-local model for cell movement:

$$u_t = D_u \Delta u - \nabla \cdot \left(u\phi \int_{S^{n-1}} \sigma f(a(x+\rho\sigma)) d\sigma \right).$$

To apply the model to chemotactic-cell movement, we must consider the generation of force in response to an external signal. Here, in the interest of model simplicity, we ignore many of the details; a comprehensive model could incorporate any number of processes, including binding of chemoattractant to cell surface receptors, internal signalling, *etc.* We take the simplest assumption: the number of focal attachments, and hence the force, generated along the membrane is directly proportional to the local chemoattractant concentration, i.e.

$$f(a(x+\rho\sigma)) \propto b(x+\rho\sigma)\,, \tag{5}$$

where b represents the concentration of attractant-bound receptors. Under the simple model for attractant-receptor binding (see Othmer and Stevens [24]), we assume

$$b = \frac{Ks}{\gamma + s} \tag{6}$$

Clearly, for sufficiently large γ, we can take $b \propto s$, leading to the non-local model

$$\begin{aligned} u_t &= D_u \Delta u - \nabla \cdot \left(u\phi \int_{S^{n-1}} \sigma s(x+\rho\sigma) d\sigma \right), \\ s_t &= D_s \Delta s + h(u,s). \end{aligned}$$

With the scaling $\phi = \frac{\chi n}{\omega \rho}$, we obtain the nonlocal system (2)-(3). This scaling is chosen to permit direct comparison with the classical chemotaxis system (1).

2.2. **Derivation from a Kinetic Transport Equation.** The nonlocal model can also be derived from a kinetic transport model, in which cells are assumed to perform a velocity jump process. The nondimensionalized master equation then has the form

$$\varepsilon^2 f_t + \varepsilon v \cdot \nabla f = T_0(f) + \varepsilon T_1(f)\,,$$

where $f(x,v,t)$ is the distribution function of cells in the position-velocity phase space, and the small dimensionless parameter ε results from a macroscopic diffusion scaling. The left hand side of the equation models movement with constant velocities, whereas the right hand side describes the velocity jumps. We consider a dominating isotropic process, where all possible post-jump velocities have the same probability:

$$T_0(f)(x,v,t) = \frac{1}{|V|} u_f(x,t) - f(x,v,t) = \frac{1}{|V|} \int_V [f(x,v',t) - f(x,v,t)] dv'\,.$$

Here V and $|V|$ denote the set of all possible velocities (assumed to be rotationally symmetric) and its measure, respectively. This is the simplest possible model. For the second process, the cell measures the chemical concentration along a sphere with radius ρ around its position x. Post-jump velocities with directions of higher chemical concentration occur with higher probability. The turning operator is given by

$$\begin{aligned} &T_1(f)(x,v,t) = \\ &\int_V \left[b\left(s\left(x + \rho \frac{v}{|v|}, t \right) \right) f(x,v',t) - b\left(s\left(x + \rho \frac{v'}{|v'|}, t \right) \right) f(x,v,t) \right] dv'\,, \end{aligned}$$

where the rate $b\,(s\,(x+\rho v'/|v'|,t))$ (b increasing) of jumping from velocity v to v' could be modelled as proportional to the concentration of bound receptors as a function of the extracellular signal s. A continuum model of Keller-Segel type can be derived by the macroscopic limit $\varepsilon \to 0$. We shall sketch the formal procedure. More details and rigorous justifications can be found in [9], [22], [5].

Obviously, the limiting distribution function is independent from the velocity: $f_0(x,v,t) = u(x,t)/|V|$ with the macroscopic cell density u, which is not determined by the limiting equation $T_0(f_0) = 0$. After dividing the transport equation by ε, we have

$$\varepsilon f_t + v\cdot\nabla f = T_0\left(\frac{f-f_0}{\varepsilon}\right) + T_1(f)\,.$$

Denoting the limit of $(f-f_0)/\varepsilon$ by R, we obtain

$$R = -v\cdot\nabla f_0 + T_1(f_0) + u_1$$

Finally, division of the transport equation by ε^2 and integration with respect to v gives the conservation equation

$$(u_f)_t + \nabla\cdot\int_V v\frac{f-f_0}{\varepsilon}dv = 0\,.$$

In the limit $\varepsilon\to 0$, the convection-diffusion equation

$$u_t + \nabla\cdot(-D_u\nabla u + uv_s) = 0\,,$$

is obtained. The diffusivity is given by $D_u = \frac{1}{n|V|}\int_V |v|^2 dv$, and the macroscopic chemotactic velocity can be computed as

$$v_s = \chi\int_{S^{n-1}} \sigma\, b\,(s\,(x+\rho\sigma,t))\,d\sigma\,, \tag{7}$$

where the constant χ results from the integral in the radial direction. For linear b, the chemotactic velocity is proportional to the nonlocal approximation of the gradient as in (2). In Section 5, numerical experiments are also carried out with a nonlinear b, modelling saturation of bound receptors.

3. **The Nonlocal Chemotaxis Model Prevents Blow-up.** The main theoretical result of this paper is global existence and uniform boundedness of solutions of (2), posed on a domain $\Omega\subset\mathbb{R}^n$ with smooth boundary, subject to initial conditions

$$u(x,0) = u_I(x)\,,\quad s(x,0) = s_I(x)\,,\qquad x\in\Omega\,, \tag{8}$$

and zero flux boundary conditions

$$n\cdot\nabla s = n\cdot(D_n u\nabla u - \chi u\,\mathring{\nabla}_\rho\, s) = 0\,,\qquad \text{on } \partial\Omega\,, \tag{9}$$

where n denotes the unit outward normal along $\partial\Omega$. We allow the whole space case $\Omega=\mathbb{R}^n$. If Ω has a boundary, it is assumed to be smooth, and ρ is assumed small enough, such that

$$\omega_\Omega(x) \geq \underline{\omega} > 0 \qquad \text{for all } x\in\Omega\,. \tag{10}$$

We denote the $L^p(\Omega)$-norm by $\|\cdot\|_p$ and start with a general lemma on convection-diffusion equations.

Lemma 1. *Let the components of the vector field $v:\ \Omega\times(0,\infty)\to\mathbb{R}^n$ be uniformly bounded, and let $u_I\in L^\infty(\Omega)\cap L^1(\Omega)$ satisfy $u_I\geq 0$. Then the solution of the initial-boundary value problem*

$$u_t=\nabla\cdot(\nabla u-uv)\,,\qquad u(t=0)=u_I\,,\qquad n\cdot(\nabla u-uv)=0\ \text{on}\ \partial\Omega\,,$$

satisfies $u\in L^\infty((0,\infty)\times\Omega)$ and

$$\sup_t\|u\|_\infty\leq C(\|u_I\|_1,\|u_I\|_\infty,\sup_t\|v\|_\infty,n)\,.$$

Proof: We start with a formal computation. For $1\leq p<\infty$, we obtain

$$\begin{aligned}\frac{d}{dt}\|u\|_p^p &= 2(p-1)\left(-\frac{2}{p}\|\nabla(u^{p/2})\|_2^2+\int_\Omega u^{p/2}v\cdot\nabla(u^{p/2})\,dx\right)\\ &\leq 2(p-1)\left(-\frac{1}{p}\|\nabla(u^{p/2})\|_2^2+\frac{p}{4}\sup_t\|v\|_\infty^2\|u\|_p^p\right)\,.\end{aligned}\tag{11}$$

Now, similarly to [2] we use the Nash inequality [20]

$$\|f\|_2^{1+2/n}\leq c_n\|f\|_1^{2/n}\|\nabla f\|_2\,,$$

with $f=u^{p/2}$ and with the abbreviation $z_p(t)=\|u(\cdot,t)\|_p^p$:

$$\frac{dz_p}{dt}\leq 2(p-1)z_p\left(\frac{p}{4}\sup_t\|v\|_\infty^2-\frac{z_p^{2/n}}{pc_n^2z_{p/2}^{4/n}}\right)\,.\tag{12}$$

This will lead to a global-in-time bound for z_p in terms of a bound for $z_{p/2}$. The strategy of the rest of the proof is to iteratively obtain bounds for z_{2^k} for all $k\in\mathbb{N}$ and to show that these bounds are uniform in k such that the result of the lemma follows by $k\to\infty$.

By interpolation, we have that

$$\|u_I\|_p\leq\|u_I\|_\infty^{(p-1)/p}\|u_I\|_1^{1/p}\leq\max\{\|u_I\|_\infty,\|u_I\|_1\}=:K\,.$$

We use induction to show that

$$z_{2^k}(t)\leq M_k,\tag{13}$$

where

$$M_k=\max\{K^{2^k},\,A2^{nk}M_{k-1}^2\},\quad M_0=K,$$

and a k-independent constant

$$A:=2^{-n}(\sup_t\|v\|_\infty c_n)^n.$$

Indeed, for $k=0$ we use $z_1\leq K$ (as a consequence of conservation of mass) and obtain from (12) that

$$\frac{dz_2}{dt}\leq 2z_2\left(\frac{1}{2}\sup_t\|v\|_\infty^2-\frac{z_2^{2/n}}{2c_n^2K^{4/n}}\right)\,.\tag{14}$$

The right hand side of (14) has two zeroes, at $z_2=0$ and $z_2=2^nAK^2$. If the initial condition $z_2(0)\geq 2^nAK^2$ then $z_2(t)\leq z_2(0)=\|u(.,0)\|_2^2\leq K^2$. If $z_2(0)\leq 2^nAK^2$ then $z_2(t)\leq 2^nAK^2$. Which proves the claim (13) for $k=1$.

Now assume (13) holds for $k-1$. Then

$$\frac{dz_{2^k}}{dt}\leq 2(2^k-1)z_{2^k}\left(\frac{2^k}{4}\sup_t\|v\|_\infty^2-\frac{z_{2^k}^{2/n}}{2^kc_n^2M_{k-1}^{4/n}}\right)\,.\tag{15}$$

The zeroes of the right hand side (15) are now 0 and $A2^{nk}M_{k-1}^2$. With the same argument as above we conclude that

$$z_{2^k}(t) \leq \max\{K^{2^k},\, A2^{nk}M_{k-1}^2\}$$

which proves the claim (13).

Again by induction it is straightforward to show that

$$K^{2^k} \leq 2^{kn}M_{k-1}^2,$$

Hence with $B = \max\{A, 1\}$, we may change the definition of the upper bounds to

$$M_k = B2^{kn}M_{k-1}^2\,, \qquad M_0 = K\,.$$

The solution of this recursion is

$$M_k = B^{2^k-1}2^{a_k n}K^{2^k}\,,$$

with $a_k = k + 2a_{k-1}$, $a_0 = 0$. Since $a_k = 2^{k+1} - k - 2 < 2^{k+1}$ and $B \geq 1$, we obtain $M_k \leq (B4^nK)^{2^k}$ and, thus, the uniform-in-k bound

$$\sup_t \|u\|_{2^k} \leq 4^n \max\{\|u_I\|_\infty, \|u_I\|_1\} \max\left\{1, (\sup_t \|v\|_\infty c_n/2)^n\right\}\,,$$

completing the proof. ∎

Theorem 1. *Let $\chi, \rho, D_u, D_s, \alpha$, and β be positive constants, let the initial data satisfy*

$$u_I \in L^\infty(\Omega) \cap L^1(\Omega)\,, \qquad s_I \in W^{1,q}(\Omega)\,,$$

with $1 < q < \frac{n}{n-1}$, and, if Ω has a boundary, let (10) hold. Then (2), (8), (9) has a global solution with

$$u \in L^\infty((0,\infty) \times \Omega)\,,$$

i.e., the cell density is uniformly bounded in position and time.

Proof: Local existence is a standard result, and global existence will be a consequence of the estimates we shall derive.

By the assumptions on the initial data and mass conservation we have $\|u\|_1 = \|u_I\|_1$. This implies (analogously to Hwang-Kang-Stevens [15]) that s is bounded in $W^{1,q}(\Omega)$ uniformly in t. By the smoothness of $\partial\Omega$, there exists an extension to $\mathbb{R}^n$ bounded in $W^{1,q}(\mathbb{R}^n)$.

The sphere S_ρ with centre in the origin and radius ρ is a smooth $(n-1)$-dimensional manifold. Therefore, by the standard result on traces, $W^{1,q}(\mathbb{R}^n)$ is continuously embedded in $W^{1-1/q,q}(S_\rho)$ and, consequently, also in $L^1(S_\rho)$ (by the boundedness of S_ρ). Therefore,

$$|\overset{\circ}{\nabla}_\rho f(x=0)| \leq c\|f\|_{W^{1,q}(\mathbb{R}^n)}$$

holds for the whole space definition (3) of $\overset{\circ}{\nabla}_\rho$. The choice $f(x) = s(x_0 + x, t)$ and the translation invariance of the $W^{1,q}(\mathbb{R}^n)$-norm imply that $\|\overset{\circ}{\nabla}_\rho s\|_\infty$ is bounded uniformly in time, again for the definition (3) of the nonlocal gradient. This immediately implies the same result for the nonlocal gradient as defined by (4), since the measure $\omega_\Omega(x)$ is bounded away from zero.

Now the proof is completed by an application of the previous lemma. ∎

Remark 1. Almost the same proof can be used for a quasistationary model for the chemoattractant, i.e., when the time derivative is cancelled in the s-equation. Instead of the result for parabolic equations from [15] a corresponding result from potential theory would have to be used. The assumption $\beta > 0$ on the decay of the chemoattractant helps, but is possibly not essential.

4. **Steady States.** In this section we investigate steady states of the non local chemotaxis model (2). We will show that steady states cannot have spike local maxima and construct approximative plateau steady states.

Steady states of the non local model (2) satisfy the equations

$$\begin{aligned} 0 &= \nabla \cdot (\nabla u - \chi u \overset{\circ}{\nabla}_\rho s) \\ 0 &= D_s \Delta s + \alpha u - \beta s, \end{aligned} \tag{16}$$

4.1. **Linear Stability Analysis in 1-D.** To compare the stability properties of the model (2) to those of the classical chemotaxis model (1) we perform a linear stability analysis at the homogeneous steady state for the one-dimensional case of (2).

A homogeneous steady state for system (16) is given by $(\bar{u}, \bar{s})$ where $\bar{s} = \alpha\bar{u}/\beta$, and $\bar{u}$ is determined by the initial population density. Linearization of (2) in 1-D at the steady state gives

$$\begin{aligned} u_t &= u_{xx} - \chi\bar{u}(\overset{\circ}{\nabla}_\rho s)_x \\ s_t &= D_s s_{xx} + \alpha u - \beta s, \end{aligned} \tag{17}$$

We use Fourier transformation to obtain the characteristic equation between eigenvalues λ and modes k. The 1-D nonlocal gradient is

$$\overset{\circ}{\nabla}_\rho s = \frac{1}{2\rho}(s(x+\rho) - s(x-\rho))$$

while its Fourier transform is given by

$$\mathcal{F}(\overset{\circ}{\nabla}_\rho s) = i\frac{\sin(k\rho)}{\rho}\mathcal{F}(s).$$

Transforming the linearized system (17), we find that the stability is determined by the eigenvalues λ of the matrix

$$A_k := \begin{pmatrix} -k^2 & k\chi\bar{u}\frac{\sin(k\rho)}{\rho} \\ \alpha & -D_s k^2 - \beta \end{pmatrix}.$$

The trace and determinant of A_k are

$$\mathrm{tr}A_k = -k^2(1+D_s) - \beta < 0 \qquad \det A_k = k^2(D_s k^2 + \beta) - \alpha\chi\bar{u}k\frac{\sin(k\rho)}{\rho}.$$

For $k = 0$ we find $\det A_0 = 0$. Hence, for $k = 0$ there exists an eigenvalue $\lambda_0 = 0$, which relates to the conservation property of (2). For a given total population we obtain instability, if we find a mode $k > 0$ for which $\det A_k < 0$. This translates into the condition

$$k(D_s k^2 + \beta) < \alpha\chi\bar{u}\frac{\sin(k\rho)}{\rho}. \tag{18}$$

Note that for $\rho \to 0$, we have $\frac{\sin(k\rho)}{\rho} \to k$. Then (18) reduces to the necessary condition for pattern formation in the classical chemotaxis model (1), i.e.

$$D_s k^2 + \beta < \alpha\chi\bar{u}. \tag{19}$$

Since for each $\rho > 0$, $\frac{\sin(k\rho)}{\rho} < k$, condition (18) for instability in the non-local model is stronger than the corresponding condition (19) for the classical model. In particular, given that (19) is satisfied, it is always possible to determine a bounded ρ_c for which no pattern formation is possible for $\rho > \rho_c$. Since $|\sin(x)| \leq 1$ we can explicitly calculate

$$\rho_c = \sup_{k>0} \left\{ \frac{\alpha\chi\bar{u}}{k(D_s k^2 + \beta)} \right\}.$$

For example, if we study (2) with homogeneous Dirichlet boundary conditions on an interval $[0, L]$, then the supremum would be obtained for $k = \pi/L$.

4.2. **Properties of the Non-Local Gradient.** The nonlocal gradient (3) has the properties that $\overset{\circ}{\nabla}_\rho s(x,t) = 0$ for constant distribution s and that for differentiable $s(x)$ we have

$$\lim_{\rho\to 0} \overset{\circ}{\nabla}_\rho s(x) = \nabla s(x).$$

It is rather useful to study the Taylor expansion of the non local gradient for small $\rho > 0$. In Hillen [8] it is shown that

$$\overset{\circ}{\nabla}_\rho s(x) = \nabla s(x) + \frac{\rho^2}{2(2+n)} \nabla(\Delta s(x)) + \mathcal{O}(\rho^4), \tag{20}$$

where n is the space dimension and Δ denotes, as usual, the Laplacian. Hence the first correction term to ∇s is of third order.

It would be interesting to study rigorously the convergence of solutions of (2) for $\rho \to 0$. In which sense, if at all, do they converge to solutions of (1)? We will not address this question here.

As shown in [8] the nonlocal gradient can be used to classify local maxima and to distinguish spikes versus plateaus.

Definition 1. (from [8]) A local maximum x_0 of $f : U \subset \mathbb{R}^n \to \mathbb{R}$ is called a

$$\begin{aligned} \textit{spike} \quad &\Longleftrightarrow \quad \exists\, \rho^* > 0 \quad \text{such that} \\ &\quad \overset{\circ}{\nabla}_\rho \left(\nabla f(x_0)\right) - \text{Hess}\left(f(x_0)\right) \quad \text{is positive} \\ &\quad \text{definite for all} \quad 0 < \rho < \rho^*, \end{aligned}$$

$$\begin{aligned} \textit{plateau} \quad &\Longleftrightarrow \quad \exists\, \rho^* > 0 \quad \text{such that} \\ &\quad \overset{\circ}{\nabla}_\rho \left(\nabla f(x_0)\right) - \text{Hess}\left(f(x_0)\right) \quad \text{is negative} \\ &\quad \text{definite for all} \quad 0 < \rho < \rho^*. \end{aligned}$$

Using the n-dimensional Taylor expansion we have proven in [8]

Theorem 2. *Assume $f \in C^5(U)$ and $\text{Hess}\left(\Delta f(x_0)\right)$ is invertible. Then*

$$x_0 \quad \textit{is a spike} \quad \Longleftrightarrow \quad \text{Hess}\left(\Delta f(x_0)\right) \quad \textit{is positive definite,}$$

$$x_0 \quad \textit{is a plateau} \quad \Longleftrightarrow \quad \text{Hess}\left(\Delta f(x_0)\right) \quad \textit{is negative definite.}$$

4.3. **No Spikes.**

Theorem 3. *Assume the steady state $u(x), s(x)$ of (2) have a common local maximum. Then this maximum cannot be a spike.*

Proof. We rewrite the first equation of (16) as

$$0 = \nabla \cdot (\nabla u - \chi u \nabla s + \chi u (\nabla s - \mathring{\nabla}_\rho\, s)).$$

Using a transformation introduced by Nanjundiah [19] we define

$$\psi = u e^{-\chi s}.$$

Then we obtain

$$\begin{aligned} 0 &= \nabla \cdot (\nabla \psi e^{\chi s}) + \chi \nabla \cdot (u(\nabla s - \mathring{\nabla}_\rho\, s)) \\ &= e^{\chi s}\Big(\Delta \psi + \chi \nabla \psi \cdot (2\nabla s - \mathring{\nabla}_\rho\, s) \\ &\quad + \chi \psi (\nabla s \cdot (\nabla s - \mathring{\nabla}_\rho\, s) + \nabla \cdot (\nabla s - \mathring{\nabla}_\rho\, s))\Big) \end{aligned} \tag{21}$$

Now we assume that u, s and ψ have a common local maximum at $x_0 \in M$, i.e.

$$\nabla\psi(x_0) = 0,\ \Delta\psi(x_0) < 0,\ \nabla u(x_0) = 0,\ \Delta u(x_0) < 0,\ \nabla s(x_0) = 0,\ \Delta s(x_0) < 0.$$

Then (21) evaluated at x_0 reduces to

$$0 = \Delta \psi + \chi \psi (\Delta s - \nabla \cdot \mathring{\nabla}_\rho\, s). \tag{22}$$

If the local maximum is a spike as defined in Definition 1, then the matrix

$$\mathring{\nabla}_\rho\, (\nabla s(x_0)) - \mathrm{Hess}(s(x_0))$$

is positive definite. This implies in particular that

$$\Delta s(x_0) - \nabla \cdot \mathring{\nabla}_\rho\, s(x_0) < 0,$$

which together with $\Delta\psi(x_0) < 0$ gives a contradiction to (22). Hence x_0 cannot be a spike.

4.4. **Approximate Plateaus.** We saw in the previous subsection that steady state solutions are not of spike type. Here we show that pattern formation still can occur in form of plateau solutions. We were not successful to explicitly find plateau solutions for the nonlocal model (16), we can, however, find approximate steady states.

For ρ small enough the nonlocal gradient can be approximated as shown in (20). We take the first two terms and define

$$\phi(x) := s + \frac{\rho^2}{2(2+n)} \Delta s$$

Then the approximate steady states on a smooth bounded domain Ω satisfy the fourth order equation

$$\begin{aligned} 0 &= \nabla \cdot (\nabla u - \chi u \nabla \phi) \\ 0 &= D_s \Delta s + \alpha u - \beta s, \end{aligned} \tag{23}$$

From this representation we see that the nonlocal gradient regularizes the same way as a fourth order term does. We study

$$\Psi = u e^{-\chi \phi}$$

and obtain

$$0 = (\Delta\Psi + \chi\nabla\Psi\cdot\nabla\phi)e^{\chi\phi}.$$

Hence Ψ satisfies a Hopf maximum principle, thus $\Psi(x)$ must be constant.

$$\Psi(x) = \Psi.$$

Since $\Psi = ue^{-\chi\phi}$ we find

$$u = \Psi e^{\chi\phi} \quad \phi = \frac{1}{\chi}(\ln u - c), \quad c = \ln\Psi.$$

The steady state system (23) becomes

$$\begin{array}{rcl} s + \frac{\rho^2}{2(2+n)}\Delta s & = & \frac{1}{\chi}(\ln u - c) \\ D_s\Delta s & = & \beta s - \alpha u, \end{array} \tag{24}$$

We use the second equation of (24) to replace Δs in the first equation, which gives

$$\begin{array}{rcl} s\left(1 + \frac{\beta\rho^2}{2(2+n)D}\right) & = & \frac{\alpha\rho^2}{2(2+n)D}u + \frac{1}{\chi}(\ln u - c) \\ D_s\Delta s & = & \beta s - \alpha u, \end{array} \tag{25}$$

For convenience we introduce

$$\kappa := \frac{\rho^2\chi}{2(2+n)D}$$

and we solve the first equation of (25) for s:

$$s = \frac{\alpha\kappa u + \ln u - c}{\chi + \beta\kappa}.$$

This expression for s is then used in the second equation of (24) to obtain a second order equation for u:

$$\Delta u\left(\alpha\kappa + \frac{1}{u}\right) - \frac{(\nabla u)^2}{u^2} = \frac{\beta}{D}\ln u - \frac{c}{D} - \frac{\alpha\kappa}{D}u. \tag{26}$$

We study the one-dimensional case on an interval $[0, l]$ with homogeneous Neumann boundary conditions in more detail. In one space dimension equation (26) can be written as a first order system

$$\begin{array}{rcl} u' & = & w \\ w' & = & \frac{Dw^2 + \beta u^2\ln u - cu^2 - \alpha\chi u^3}{D(\alpha\chi u^2 + u)} \end{array} \tag{27}$$

with boundary conditions

$$w(0) = 0 \qquad w(l) = 0.$$

The steady states of (27) satisfy $w = 0$ and $u = 0$ or

$$\beta\ln u - c - \alpha\chi u = 0. \tag{28}$$

The equation (28) has zero, one or two roots. In a systematic analysis of all cases (not shown here) it turns out that only the case of three roots gives non-trivial steady states. In Figure 1 we show an example for $D = 1, \mu = 0.12, \beta = 1, \nu = 1, \kappa = 10$. In Figure 1 (a) the vectorfield of (27) is shown and in Figure 1 (b) typical nontrivial plateau steady states are shown in the phase plane.

Note that for $\rho \to 0$ equation (28) becomes $\beta\ln u = c$, hence it has exactly one root at $u = \psi e^{\beta}$. The third root diverges to ∞ and the plateau steady states disappear.

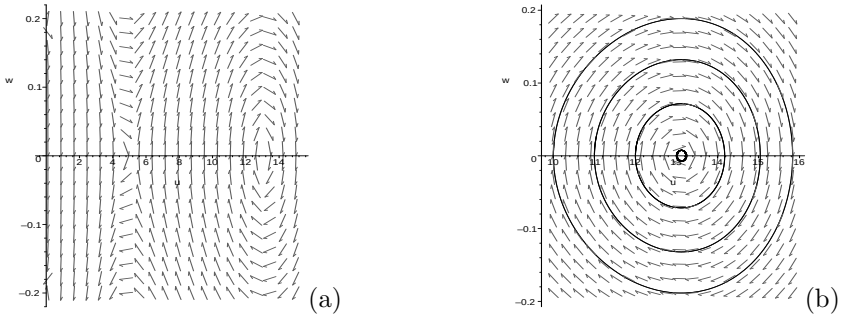

FIGURE 1. (a) The vectorfield for the case of three roots of the equation (28). (b) Plateaus solutions appear as closed circles around the third equilibrium point.

5. **Numerical Results.**

5.1. **Numerical Method.** We turn our attention to numerical solutions of the non-local chemotaxis model. The right-hand sides of the system (2) are discretised in conservative flux form, employing a second order central differencing scheme for the diffusion terms and a high order upwinding method with a Koren flux limiting function for the advective term. The conservative flux form is appropriate for the diffusion-advection equation, as it ensures mass conservation ([14]). Flux limiting allows higher order upwinding for the advective term, while maintaining positivity of solutions. The direction for the upwinding depends on the sign of the non-local term in the advective component, calculated at the boundary between adjacent mesh points. In one dimension, it is thus necessary to calculate concentration data at $c(x_b \pm \rho)$, where x_b denotes the midpoint between adjacent mesh points. We approximate $c(x_b \pm \rho)$ by linear interpolation using the nearest two mesh points. The two-dimensional problem is solved analogously, yet determining the non-local term now requires calculation of the integral on a circle of radius ρ, centred on the mid-point between adjacent mesh points. We approximate this by discretising the circle into a lattice of surface grid points, and employing linear interpolation from the surrounding domain grid points to give cell/chemical densities at the surface grid points. Time integration is carried out using an explicit trapezoidal scheme; investigations into higher order schemes (e.g. 4th order Runge-Kutta) yielded little difference. More efficient time integration techniques, for example applying "operator-splitting" and using distinct methods (e.g. implicit, explicit) to each right hand side term should be investigated in a more extensive numerical study.

For simplicity in calculating the non-local terms, we set periodic boundary conditions; biologically relevant boundary conditions (e.g. Dirichlet or zero-flux) can also be applied, yet one must pay appropriate attention to the non-local term near the boundaries (see (4)) . To determine the approximate accuracy of the solver, a series of test simulations were performed and compared against a "reference" solution computed on a highly refined grid. Calculations determined our scheme to be approximately second order accurate in space.

5.2. **Aggregation Results.**

5.2.1. *1D Numerics.* In Figure 2 we show the results of a typical simulation of the 1D non-local model. Parameters have been selected such that the instability

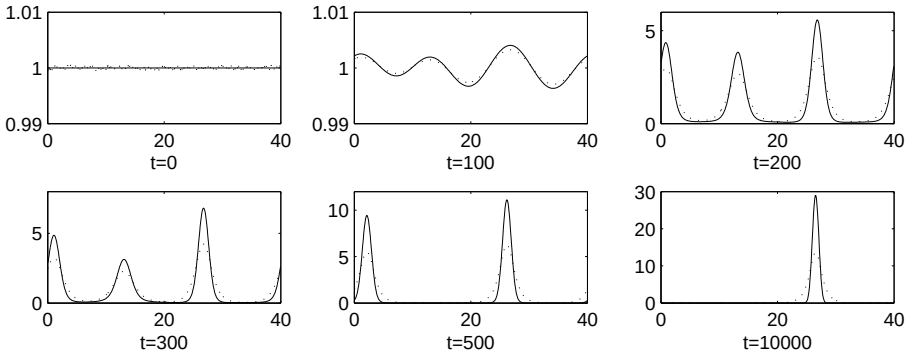

FIGURE 2. Evolving cell (solid) and chemical (dotted) profiles for the 1D non-local model. The following parameters are chosen: $D_u = D_s = \alpha = \beta = 1.0$, $\rho = \chi = 2.0$ on a domain $[0, 40]$ with periodic boundary conditions. We initially set $u(x, 0) = 1.0$ and a small random perturbation of the homogeneous steady state for the chemical concentration. 401 mesh points are used for the grid.

condition, (18), is satisfied. The numerics demonstrate the formation of multiple cell aggregations, which subsequently undergo a coarsening process until a single peak remains. This behaviour is analogous to that observed in Keller-Segel type models of chemotaxis (e.g. see [25]).

To demonstrate the effect of the sampling radius, we simulate the model over a range of ρ. For $\rho \to 0$, the non-local model reduces to the classical Keller-Segel model (1) and we plot solutions for this case in Figure 3 (a) for comparison. Numerical simulations at small ρ, Figure 3 (b) demonstrate a predictably close match. Increasing the radius results in a lower peak/broader aggregation, (c)-(f). It is possible to use condition (18) to determine the critical value for ρ above which patterning is no longer possible. The lowest non-zero mode k satisfying the boundary conditions is $k = 2\pi/L$, where L is the domain length. Substituting this, together with the parameters listed in Figure 3, into (18) we determine $\rho_c = 2.2552$ to 4 d.p. This value is both confirmed by and validates the accuracy of the numerical simulations: for $\rho_c = 2.255$ an aggregation (albeit small) eventually develops, Figure 3 (g), while an increase of ρ_c to 2.256 results in no pattern formation, (h).

5.2.2. *2D Numerics.* We extend the numerical analysis to two dimensions. In 2D the classical Keller-Segel model is known to exhibit finite time blow-up (for suitable initial data). A typical scenario is shown in Figure 4 (a): already at $T = 13.8$ the cell density is highly concentrated, and the solution can no longer be computed (numerical blow-up). In Figures 4 (b)-(e) we plot cell density profiles under different ρ for the non-local model. The global existence result for the non-local model is confirmed by the numerics: inclusion of a sampling radius prevents blow-up and allows solutions to evolve to a heterogeneous steady state solution. The 2D numerics parallel the 1D observations: decreasing ρ results in a concentrated solution and a plot of the maximum density vs ρ appears consistent with convergence to a blow-up solution as $\rho \to 0$, Figure 4 (f). Increasing ρ results in a dispersed peak and above some critical radius ρ_c aggregation is no longer possible Figure 4 (e) .

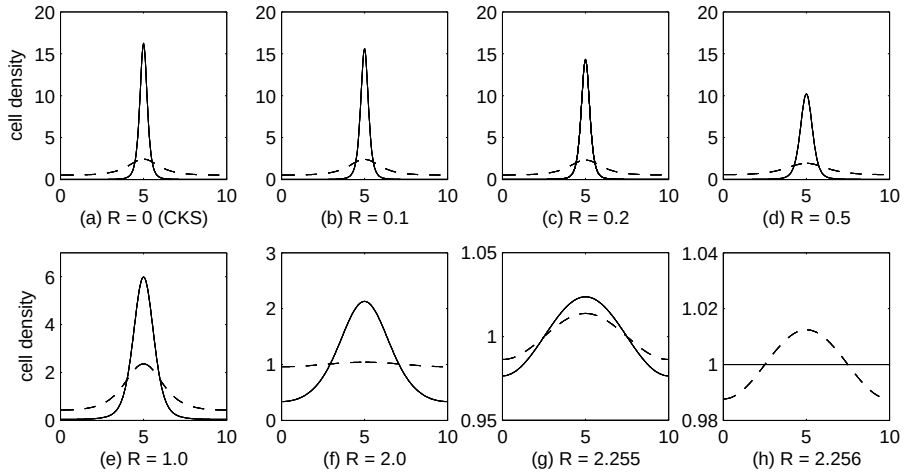

FIGURE 3. Intermediate (dashed) and long term (solid) cell density profiles for the non-local model under various ρ: (a) $\rho = 0$, corresponding to the classical Keller-Segel model, at times $T = 30$ and 200; (b) $\rho = 0.1$ at $T = 30, 200$; (c) $\rho = 0.2$ at $T = 30, 200$; (d) $\rho = 0.5$ at $T = 30, 200$; (e) $\rho = 1.0$ at $T = 40, 500$; (f) $\rho = 2.0$ at $T = 40, 500$; (g) $\rho = 2.255$ at $T = 1000, 200000$; (h) $\rho = 2.255$ at $T = 1000, 200000$. Parameter values as for Figure 2 on a domain $[0, 10]$ (201 mesh points). Initial conditions are $u(x, 0) = 1.0$, $v(x, 0) = 0.95 + 0.1 \exp(-0.1(x - 5)^2)$.

In Figure 5 we plot solutions on a larger initial domain; here initial conditions consist of a random spatial perturbation from the homogeneous steady state. Simulations indicate pattern formation, with a number of cell aggregations emerging at (roughly) equally spaced locations. Altering the sampling radius alters both the density of the peak, but also the number of the aggregations to emerge.

5.3. **Model Variations.** The numerical results above confirm the earlier analysis: critically, we observe global existence for the non-local model (2) with (3). This formulation of the model relates to a precise set of assumptions stipulated during the derivation. To indicate whether the inclusion of the non-local term allows global existence for more general formulations, we numerically solve some model variants.

5.3.1. *Incorporation of Receptor Binding.* During the derivations of the model, linear functions were chosen to describe key processes for simplicity. More plausible, nonlinear forms, can also be chosen; for example by taking a saturating dependence on the signal concentration (i.e. of the form (6) in (5) or in (7)), we derive the following non-local term:

$$\int_{S^{n-1}} \sigma \frac{s(x + R\sigma, t)}{k + s(x + R\sigma, t)} \, d\sigma.$$

Replacing the integral term in equation 3 with the above still allows pattern formation, albeit with a less concentrated peak, Figure 6 (a).

5.3.2. *Non-Diffusing Scenarios.* Tactic responses to non-diffusing substances can occur in a number of instances. "Haptotaxis", for example, describes cell movement along gradients of adhesion molecules tightly bound to a rigid extracellular matrix. Non-diffusing chemical species in classical chemotaxis models often create greater numerical challenges: steeper gradients develop and blow-up can occur even in 1D. Numerics indicate that the non-local term resolves such difficulties, and solutions still appear to exist globally Figure 6 (b).

6. **Discussion.** In this paper we introduced a non-local gradient sensing term into the classical chemotaxis equations. We have proven that solutions to the non local model exist globally in time, on bounded and unbounded domains, independent of the space dimension.

The explicit incorporation of a non-local sampling radius for the cell response to its environment provides a new level of detail for describing cell migration in response to external cues. In this paper, we have explored the general property of solutions to the model including its ability to exhibit pattern formation, the global existence of solutions and the nature of the steady states. We have seen that, as $\rho \to 0$, the solutions become higher and steeper and finally blow-up for $\rho = 0$. In addition, plateau steady states cease to exist for $\rho = 0$.

Numerical simulations of the model indicated the global existence properties of the non-local model may extend to even stronger cases than that determined theoretically in Section 3. For example under zero-diffusion of the chemical species, a case that leads to blow-up even in 1D for the classical chemotaxis model, steady state patterns still develop (Figure 6 (b)). This result remains to be demonstrated analytically.

While this paper has not had a specific biological application in mind, it is necessary to consider the use of the model in specific biological processes. The explicit incorporation of a non-local sampling radius, with its length scale of cell diameters, limits the ability to perform numerical explorations at "truly macroscopic scales" (for example, the size of large tissues/organs or *Dictyostelium* and bacteria aggrgations). Thus, this model may be most appropriate at a "mesoscopic-level" - i.e. where the length scales of movement are not "hugely" greater than the size of individual cells, but when a macroscopic approach is still desirable. Two such applications include the formation of vascular patterns, or the invasion of tumour cells into surrounding tissue. An open question is thus raised as to whether it is possible to derive fully macroscopic models (i.e. PDE models) which retain the important characteristics of the non-local sampling radius. A clue to one approach for this may lie in the Taylor Expansion of the non-local term, Equation (20). While applying the first non-zero term in this expansion leads straight to the classical Keller-Segel model, using the first two non-zero terms adds a fourth order dissipative term.

REFERENCES

[1] M. Aida, K. Osaki, T. Tsujikawa, A. Yagi, and M. Mimura. Chemotaxis and growth systems with singular sensitivity function. *Nonlin. Anal. Real World Appl.*, 6:323–336, 2005.
[2] A. Arnold, P. Markowich, and G. Toscani. On large time asymptotics for drift-diffusion-poisson systems. *Transport Theory Statist. Phys.*, 29:571–581, 2000.
[3] H.C. Berg and E.M. Purcell. Physics of chemoreception. *Biophys. J.*, 20(2):193–219, 1977.
[4] P. Biler. Local and global solvability of some parabolic systems modelling chemotaxis. *Advances in Math. Sci. and Appl.*, 8(2):715–743, 1998.

[5] F. Chalub, P.A. Markowich, B. Perthame, and C. Schmeiser. Kinetic models for chemotaxis and their drift-diffusion limits. *Monatsh. Math.*, 142:123–141, 2004.
[6] Y. Dolak and C. Schmeiser. The Keller-Segel model with logistic sensitivity function and small diffusivity. *SIAM J. Appl. Math.*, 66:286–308, 2005.
[7] J. Dolbeault and B. Perthame. Optimal critical mass in the two-dimensional Keller-Segel model in $\mathbb{R}^2$. *C. R. Math. Acad. Sci. Paris*, 339:611–616, 2004.
[8] T. Hillen. A classification of spikes and plateaus. *SIAM Reviews*, 2006. to appear.
[9] T. Hillen and H.G. Othmer. The diffusion limit of transport equations derived from velocity jump processes. *SIAM J. Appl. Math.*, 61(3):751–775, 2000.
[10] T. Hillen and A. Potapov. Global existence for the classical chemotaxis model in $1-D$. *Math. Meth. Appl. Sci.*, 27:1783–1801, 2004.
[11] D. Horstmann. Lyapunov functions and L^p-estimates for a class of reaction-diffusion systems. *Coll. Math.*, 87:113–127, 2001.
[12] D. Horstmann. From 1970 until present: The Keller-Segel model in chemotaxis and its consequences I. *Jahresberichte der DMV*, 105(3):103–165, 2003.
[13] D. Hortsmann and M. Winkler. Boundedness vs. blow-up in a chemotaxis system. *J. Diff. Eq.*, 215:52–107, 2005.
[14] W. Hundsdorfer and J.G. Verwer. *Numerical Solution of Time-Dependent Advection-Diffusion-Reaction Equations*, volume 33 of *Springer Series in Computational Mathematics*. Springer-Verlag, Berlin, 2003.
[15] H.J. Hwang, K. Kang, and A. Stevens. Drift-diffusion limits of kinetic models for chemotaxis: a generalization. *Discrete Contin. Dyn. Syst. Ser. B*, 5:319–334, 2005.
[16] E.F. Keller and L.A. Segel. Initiation of slime mold aggregation viewed as an instability. *J. Theor. Biology*, 26:399–415, 1970.
[17] M. Luca, A. Chavez-Ross, L. Edelstein-Keshet, and A. Mogilner. Chemotactic signaling, microglia, and Alzheimer's disease senile plaques: is there a connection? *Bull. Math. Biol.*, 65(4):693–730, 2003.
[18] M.R. Myerscough, P.K. Maini, and K.J. Painter. Pattern formation in a generalized chemotactic model. *Bull. Math. Biol.*, 60(1):1–26, 1998.
[19] V. Nanjundiah. Chemotaxis, signal relaying and aggregation morphology. *J. Theoretical Biology*, 42:63–105, 1973.
[20] J. Nash. Continuity of solutions of parabolic and elliptic equations. *Amer. J. Math.*, 80:931–954, 1958.
[21] K. Osaki and A. Yagi. Finite dimensional attractor for one-dimensional Keller-Segel equations. *Funkcialaj Ekvacioj*, 44:441–469, 2001.
[22] H.G. Othmer and T. Hillen. The diffusion limit of transport equations II: Chemotaxis equations. *SIAM J. Appl. Math.*, 62(4):1122–1250, 2002.
[23] H.G. Othmer and P. Schaap. Oscillatory CAMP signaling in the development of dictyostelium discoideum. *Comments on Theor. Biol.*, 5:175–282, 1998.
[24] H.G. Othmer and A. Stevens. Aggregation, blowup and collapse: The ABC's of taxis in reinforced random walks. *SIAM J. Appl. Math.*, 57:1044–1081, 1997.
[25] K. Painter and T. Hillen. Volume-filling and quorum-sensing in models for chemosensitive movement. *Canadian Appl. Math. Quart.*, 10(4):501–543, 2002.
[26] K.J. Painter, H.G. Othmer, and P.K. Maini. Stripe formation in juvenile pomacanthus via chemotactic response to a reaction-diffusion mechanism. *Proc. Natl. Acad. Sci. USA*, 96:5549–5554, 1999.
[27] E.F. Pate and H.G. Othmer. Differentiation, cell sorting and proportion regulation in the slug stage of Dictyostelium discoideum. *J. Theor. Biol.*, 118(3):301–319, 1986.
[28] C.S. Patlak. Random walk with persistence and external bias. *Bull. Math. Biophys.*, 15:311–338, 1953.
[29] W.J. Rappel, P.J. Thomas, H. Levine, and W.F. Loomis. Establishing direction during chemotaxis in eukaryotic cells. *Biophysical Journal*, 83:1361–1367, 2002.
[30] J. Renclawowicz and T. Hillen. Analysis of an attraction-repulsion chemotaxis model. *submitted*, 2006.
[31] M.A. Rivero, R.T. Tranquillo, H.M. Buettner, and D.A. Lauffenburger. Transport models for chemotactic cell populations based on individual cell behavior. *Chem. Eng. Sci.*, 44:1–17, 1989.
[32] T. Suzuki. *Free Energy and Self-Interacting Particles*. Birkhäuser, Boston, 2005.

[33] R. Tyson, S.R. Lubkin, and J.D. Murray. A minimal mechanism for bacterial pattern formation. *Proc. R. Soc. London B*, 266:299–304, 1999.
[34] B.J. Varnum-Finney, E. Voss, and D.R. Soll. Frequency and orientation of pseudopod formation of Dictyostelium discoideum amebae chemotaxing in a spatial gradient: further evidence for a temporal mechanism. *Cell Motil. Cytoskeleton*, 8(1):18–26, 1987.
[35] D. Wrzosek. Long time behaviour of solutions to a chemotaxis model with volume filling effect. *Proc. Roy. Soc. Edinburgh Sect. A*, 136:431–444, 2006.

E-mail address: thillen@ualberta.ca, painter@ma.hw.ac.uk, christian.schmeiser@univie.ac.at

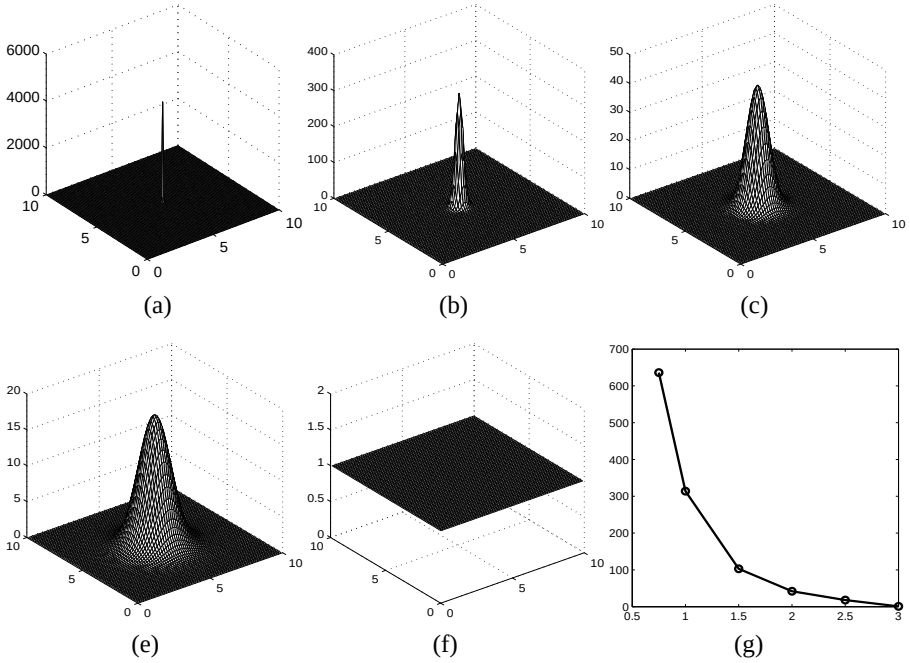

FIGURE 4. (a) Numerical simulation of the classical Keller-Segel model ($\rho = 0$). Simulation shown at $t = 13.8$, just prior to "numerical blow-up". (b)-(e) Steady state cell density patterns for the non-local model for increasing ρ: (b) $\rho = 1.0$, $T = 100$ (c) $\rho = 2.0$, $T = 150$ (d) $\rho = 2.5$, $T = 300$, (e) $\rho = 3.0$, $T = 300$. (f) Plot showing peak cell density as a function of ρ. Model parameters as for Figure 2 on the domain $[0, 10] \times [0, 10]$ (75 by 75 grid points used). Initial conditions are $u(x, y, 0) = 1.0$ and $s(x, y, 0) = 0.5 + e^{-0.5((x-5)^2+(y-5)^2)}$ on the domain $[0, 10] \times [0, 10]$.

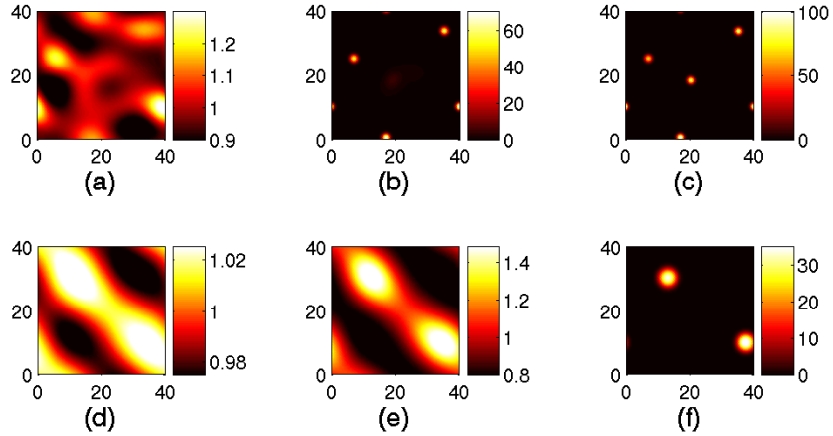

FIGURE 5. Top row: cell density evolution for $\rho = 3.0$ for (a) $t = 100$, (b) $t = 150$ (c) $t = 200$. Bottom row: cell density evolution for $\rho = 6.0$ for (d) $t = 200$, (e) $t = 300$ (f) $t = 400$. Parameters as for figure 2 on the domain $[0, 40] \times [0, 40]$ (100×100 mesh points). Initially we take $n(x, y, 0) = 1$ and a random perturbation about the homogeneous chemical concentration.

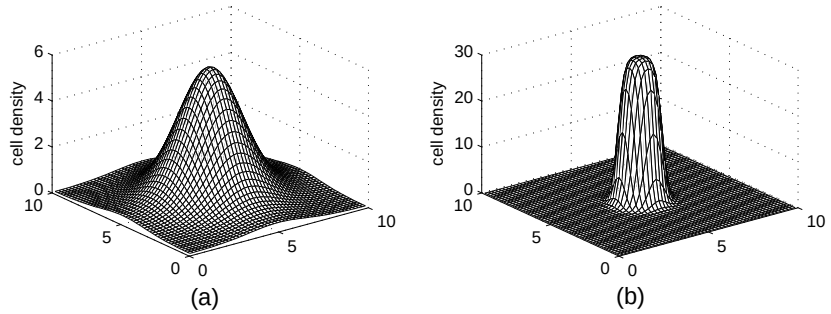

FIGURE 6. Asymptotic cell density for two model variations: (a) "receptor-binding" non-local term; (b) non-diffusion of the chemical species. Model parameters and initial conditions as for Figure 2 except in (a) where $\chi = 8$ and $k = 1$ and (b) where $D_s = 0$. Simulations solved on a domain $[0, 10] \times [0, 10]$ with 51 by 51 grid points.